MuSIC: Multi-Sequential Interactive Co-Registration for Cancer Imaging Data based on Segmentation Masks

Tanja Eichner[1,2,*] , Eric Mörth[1,3,*] , Kari S. Wagner-Larsen[1,4] , Njål Lura[1,4] ,
Ingfrid S. Haldorsen[1,4] , Eduard Gröller[2] , Stefan Bruckner[1,3] , Noeska N. Smit[1,3]

[1]Mohn Medical Imaging and Visualization Centre, Haukeland University Hospital, Norway
[2]Faculty of Informatics, TU Wien, Austria
[3]Department of Informatics, University of Bergen, Norway
[4]Department of Clinical Medicine, University of Bergen, Norway
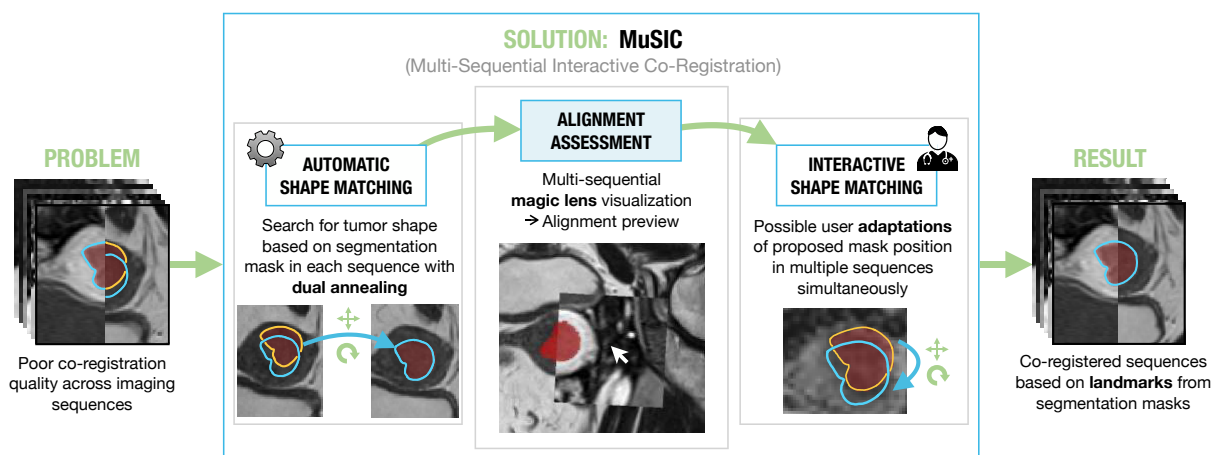∗ These authors contributed equally to this work.

Figure 1: *Proposed workflow of the MuSIC application that combines automated and interactive visual co-registration.*

Abstract

In gynecologic cancer imaging, multiple magnetic resonance imaging (MRI) sequences are acquired per patient to reveal different tissue characteristics. However, after image acquisition, the anatomical structures can be misaligned in the various sequences due to changing patient location in the scanner and organ movements. The co-registration process aims to align the sequences to allow for multi-sequential tumor imaging analysis. However, automatic co-registration often leads to unsatisfying results. To address this problem, we propose the web-based application MuSIC (Multi-Sequential Interactive Co-registration). The approach allows medical experts to co-register multiple sequences simultaneously based on a pre-defined segmentation mask generated for one of the sequences. Our contributions lie in our proposed workflow. First, a shape matching algorithm based on dual annealing searches for the tumor position in each sequence. The user can then interactively adapt the proposed segmentation positions if needed. During this procedure, we include a multi-modal magic lens visualization for visual quality assessment. Then, we register the volumes based on the segmentation mask positions. We allow for both rigid and deformable registration. Finally, we conducted a usability analysis with seven medical and machine learning experts to verify the utility of our approach. Our participants highly appreciate the multi-sequential setup and see themselves using MuSIC in the future.

CCS Concepts

• Applied computing → Health informatics; • Human-centered computing → Visualization design and evaluation methods;

1. Introduction

Endometrial cancer is the most common gynecologic cancer type in high-income countries and is one of the leading causes of cancer deaths worldwide [HS16, HSG*13, MLC*16]. Diagnostic imaging data often includes different modalities, e.g., computed tomography (CT) or MRI, per patient and examination date, depending on the body area and tumor type. This variety of medical images allows for examining varying tumor characteristics that become visible in the different modalities [LSBP18]. Radiomic tumor pro-

filing extracts meaningful tumor features from high-dimensional multi-modal imaging data with the aim of finding new imaging biomarkers. These may improve prognostication to tailor therapy [MWLH*20]. In addition, radiomic tumor profiling in endometrial cancer is promising to predict death by disease and may aid personalized treatment [Fas18, HHD*21, Ber16, HS16]. Furthermore, machine learning algorithms for automated tumor segmentation may allow for expedited radiomic tumor profiling [Hod21].

To use multiple modalities in further processing steps such as segmentation and radiomic tumor profiling, all images of a single patient have to be aligned after the acquisition, which is referred to as co-registration [MWLH*20, MBSK16]. Co-registration can account for organ movements, such as bladder filling in the pelvic area between the scans, the possible variation in the patient's location in the scanner, and the acquisition angle. Registration and segmentation belong to the biggest challenges in medical imaging with substantial potential clinical impact [SDP13]. Machine learning algorithms are currently state-of-the-art for many registration and segmentation problems and often lead to remarkable results. Still, scanning artifacts such as noise due to patient movement or low resolution, lacking training data due to anatomical variation, and physiological changes make these tasks challenging [RS14]. These factors often lead to insufficient registration and segmentation results.

Our collaborators encounter some of these unsatisfying co-registration results in endometrial and cervical cancer MRI data. Currently, the data sets are registered based on the DICOM header data that contains information regarding the patient's position in the MRI scanner. Available command-line tools that aim to align several sequences did not yield sufficient registration results in all cases and need specific settings depending on both the patient and sequence. Furthermore, existing interactive tools do not allow for multi-sequential processing. Different approaches try to automatically find insufficient co-registrations results, one example was presented by Mörth et al. [MEH*22]. These cases can then be registered, for example using landmark-based approaches which are among the most accurate ones. However, landmarks are challenging to set in cancer imaging data. For example, the tumor might appear differently in the sequences due to imaging physics, and the sequences might show low contrast and noise in the area of interest [PMEM16, FW01]. To facilitate interactive co-registration of cancer imaging data where automatic registration methods do not lead to satisfying results, we propose the MuSIC (Multi-Sequential Interactive Co-registration) approach. Our workflow is based on a pre-defined tumor segmentation mask per patient that matches one of the sequences. The mask is specified manually, or generated using machine learning approaches [Hod21]. Our main contributions are the following:

- We present interactive multi-sequential co-registration for cancer imaging data based on a segmentation mask.
- We enable automatic shape matching as a first fit and manual shifting of the segmentation mask in multiple sequences simultaneously.
- We introduce an interactive magic lens visualization presenting an alignment preview.
- We integrate co-registration based on landmarks determined

from the segmentation mask shift to allow for fast and accurate co-registration within one application.

To show the utility of our approach, we evaluated our application with five experts in gynecological cancer imaging research and two machine learning experts, using the System Usability Scale (SUS) [Bro04] and a qualitative evaluation form.

2. Related Work

The survey of Maintz et al. [MV98] introduces basic concepts regarding medical image registration and reviews existing approaches based on a broad classification scheme. We present related work based on individual steps in our workflow and differentiate between automatic and interactive registration.

Automatic Shape Matching Our registration approach is based on the alignment of tumor segmentations in two imaging sequences. To identify the tumor or another structure of interest in an image, existing approaches apply various segmentation methods to segment a target structure independently in various sequences and register them in a deformable manner. Segmentations can be generated based on shape modeling with prior information [KDSU*16], active contours [SFF06, PMWH05], level sets [TYW*03], or deep learning [XN19, CKMK19]. Several deformable registration approaches have been proposed in the field of image-guided surgery [CKMK19, KDSU*16] or cardiac imaging [TA13] to account for organ movements. In contrast to existing approaches, we search for the exact shape of a given segmentation mask in each sequence and use the single voxels as landmarks for both rigid and deformable registration.

Automatic Registration Many approaches have been published that aim for completely automated registration. For example, Fu et al. [FLW*20], as well as Haskins et al. [HKY20] provide a review regarding the use of deep learning for medical image registration. Deep learning approaches focus either on learning the similarity metric [CZZ18, SGBM*16] or learning transformation parameters [CW18, KK19, SZ18]. Ferrante et al. [FOGM18] apply transfer learning to improve the generalization of mono-modal registration algorithms to new medical domains. In addition, some methods incorporate landmarks to improve automated registration [Mah18, VLM*17]. Apart from deep learning approaches, several publicly available command-line tools for image registration require the user to specify different parameters based on the data set [ATS09, KSM*09, JBB*12]. Solving a registration problem involves many parameters that depend on the body area, contrast, and image noise, especially in multi-modal and deformable registration [MV98, SDP13, HKY20]. Therefore, the required settings for command-line tools can differ between patients and sequences. Finding a setup for each patient or sequence individually is time-consuming, as experienced by our collaborators in our endometrial cancer data set. Supervised learning requires an extensive and high-quality ground truth data set for sufficient robustness [HKY20]. However, ground truth data in registration is often lacking, as in our case of endometrial cancer imaging. We need a way to correct the results interactively for cases where automated methods fail.

Interactive Registration Several approaches provide interactive registration methods for medical imaging data to overcome the limitations of automated algorithms. Among those methods, interactive 3D registration tools have been proposed [SHS*14, LXN*05]. Smit et al. [SHS*14] offer 3D interactive manual, landmark-based, and automatic transformations, and, as well as Li et al. [LXN*05], assign a color to each volume during the rigid registration process to make them easily identifiable. The color homogeneity is then used as a similarity measure, assuming that homogeneous regions are well aligned. In the tool FireVoxel [MR], the user can choose a region of interest where the registration will be more accurate than in outer areas. The publicly available tool 3D Slicer [PHK04] offers several modules for image registration such as automatic and interactive landmark-based registration between two images. Also, Cheung et al. [CK09] let users set different landmarks during an iterative registration procedure. Setting manual landmarks is often used to assess registration accuracy. Especially in deformable registration, many landmarks are necessary, which involves much manual work. Furthermore, it can be challenging to identify anatomical landmarks in data that show low contrast or noise in areas of interest [PMEM16, FW01]. We propose to use a segmentation mask that acts as a set of pre-defined landmarks that can be placed interactively. In the aforementioned approaches, it is possible to register exactly one image volume to another. In contrast, our approach allows for the visualization and processing of multiple sequences simultaneously.

Visual Registration Evaluation Visualization methods allow for validating outcomes of individual cases qualitatively [SFJ*16]. In several approaches, checkerboards are used to assess the alignment of two images [HBR*17, CK09, PHK04]. Handels et al. [HWS*07] color-encode the displacement vector field's magnitude and displayed the result on a 3D surface model. This gives information about the deformation amount but not the registration accuracy. Schlachter et al. [SFJ*16] visualize mono-modal voxel-wise dissimilarity. Lawonn et al. [LSBP18] review approaches for multimodal data visualization, where focus-and-context visualizations play an important role. Lens visualizations represent an interactive method to examine different data characteristics. As introduced by Bier et al. [BSP*93], the view of the data is altered within a specific area. Magic lenses have been applied to the medical field, for example in volume visualization for surgical applications [KYWH12], comparative CT parameter studies [MHG10], blood flow visualization [GNBP11], or comparative visualization of MRI follow-up data [Dzy13]. In contrast to simple transparent overlays, the advantage of checkerboards is that they are applicable to show similarity even if the gray value ranges of the modalities differ. However, it is more challenging to assess registration inaccuracies in homogeneous regions [SFJ*16]. Furthermore, the accuracy assessment is limited to a pre-defined grid. Therefore, in contrast to previous approaches, we use a magic lens to compare multiple sequences to allow for interactive and localized alignment assessment.

3. Data and Requirements

In the data set from our collaborating cancer imaging researchers, seven different MR sequences with varying parameters are available per patient. The MRI sequences and parametric maps included are T2, contrast-enhanced VIBE (T1-weighted sequence),

the apparent diffusion coefficient (ADC), diffusion-weighted magnetic resonance imaging (b1000), peak enhancement (PE), time to peak (TTP), and area under the peak enhancement curve (AUC). PE, TTP, and AUC are derived from a dynamic contrast-enhanced (DCE) diffusion image and thus represent the same acquisition time point. We refer to the different MR image series as sequences.

Shifts in Imaging Sequences MRI investigations are a rather slow scanning method and may take between 30 and 60 minutes depending on the area of the body being scanned. A crucial aspect of high imaging quality is that the screened person remains still during the scanning procedure. Movements can result in image misalignment between sequences acquired at different time points. Typical movements are translation and rotation, as the scanned person may shift up, down, left, and right within the scanner. Rotation happens when the hip is tilted. The endometrium and other tissues surrounding the tumor are soft tissues. Therefore, bowel movement and bladder filling during the MRI scanning procedure can cause variations in the shape of these structures. In contrast, tumorous tissue is rigid and does not change shape during the investigation. The position of the tumor can in our case therefore only vary in translation and rotation parameters [ZRC*20, AGM17].

Automatic Co-Registration Our collaborators performed an initial automatic co-registration using FMRIB's Linear Imaging Registration Tool (FLIRT) [JBBS02] without optimization and only performing geometric alignment using scanner coordinates. However, the quality of the results varies and the algorithm does not always find an optimal solution. Our collaborators are currently working on machine learning-based approaches, but the results are still insufficient for some cases. Therefore, our collaborators are in need of an intuitive way to investigate such cases and fix the co-registration issues with the least possible amount of human interaction.

Requirement Analysis Based on the nested model for visualization by Munzner [Mun09], we characterized the problem domain. We consulted with our collaborating experts in gynecological cancer imaging and machine learning research to identify relevant challenges. We found that radiomic tumor profiling is currently used in a research setting, but the latest research suggests that it might also be essential for clinical practice soon [Fas18, HHD*21, Ber16, HS16]. Radiomic tumor profiling over multiple sequences while only having the segmentation mask available for one of them is only possible with co-registered data. As of now, the gynecological cancer imaging experts did not perform co-registrations. The machine learning experts worked with automatic solutions that do not yield satisfying results and found that landmark-based registration methods are not sufficiently intuitive to be used by radiologists. Based on our analysis, we formulated the following requirements for our application together with collaborating experts:

- R1: Automatic co-registration methods should be applied where possible
- R2: Co-registration should be easy and intuitive, targeted toward medical researchers
- R3: Quality checking capabilities for registration results should be included

Figure 2: *Main view with three orthogonal slicing directions in a T2 sequence and active magic lens visualization showing the reference sequence before processing.*

- R4: Efficient processing and visualization of multiple sequences at the same time
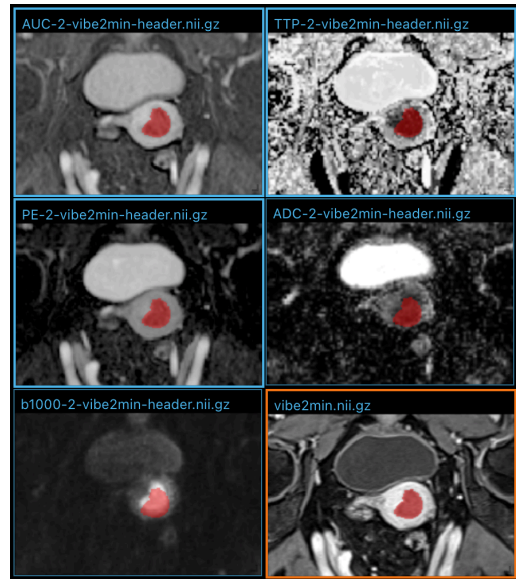- R5: The application should be deployable in a medical research setting

By satisfying these requirements, our application can be an essential asset enabling further research in exploring and analyzing imaging biomarkers for cancer research. This could enable more personalized treatment and the best possible outcome for patients.

4. MuSIC Workflow and Interface

In Figure 1, the workflow of MuSIC is illustrated. The workflow consists of an automatic shape matching (ASM) step that aims to find a suitable position of the segmentation mask, an interactive magic lens visualization for alignment assessment, interactive shape matching (ISM) for adjustments, and finally, the co-registration itself. We implemented MuSIC as a web-based application to allow for easy deployment (R5). Furthermore, the application allows for processing of all sequences of one patient at once (R4). Therefore, all the steps of the proposed workflow can be conducted within the application (R2).

User Interface The user interface is divided into a toolbar, the main view that shows one of the sequences in three slicing directions (see Figure 2), and a grid view with the remaining sequences shown in one slicing direction (in our case: axial oblique, the direction in which the sequence has been acquired, see Figure 3) (R4). This way, we provide sequence details on demand while avoiding visual overload. In addition, the grid view is further customizable in size and location of sequences.

Initially, the user uploads the desired sequences and the segmentation mask. User interaction with the slices is based on the interaction methods available in a standard radiology workstation, i.e., scrolling, zooming, and panning (R2, R5). Before starting the automatic shape matching (ASM), the user sets a reference sequence on which the segmentation mask is based and groups derived sequences that should be processed together (R4). In our data set, the same transformations should be applied to the derived sequences (PE, TTP, AUC), as they represent the same acquisition time point.

Figure 3: *Grid view with six sequences. The three sequences with the bright blue outline are grouped for simultaneous processing. The sequence on the bottom right (VIBE) is selected as reference sequence as indicated by the orange outline.*

4.1. Automatic Shape Matching

We propose a method to automatically align the segmentation mask of the reference sequence with the actual tumor borders in the other sequences, for which no mask is defined (R1). Since the tumor is a rigid structure in our context, we search for the tumor by adapting rotation and translation parameters minimizing a cost function.

Pre-Processing To limit the search space, we crop the images to the area around the original segmentation with a search margin of 15 voxels in each image direction, as determined by our medical collaborators. A larger shift is unlikely to occur. We then apply adaptive histogram normalization with 512 bins and a Gaussian Gradient Magnitude (GGM) filter with $\sigma = 1$ voxel to enhance the contrast. We determined these values heuristically. Since the contrast around the tumor is very low in some sequences, we define two values for each sequence by visual analysis to trim the histogram of the equalized volume to a specific range. These values need to be defined only once for the data set. Sequences that have been grouped by the user are processed by adding them up before applying the other pre-processing steps (R4). Histogram trimming is not necessary in this case, as the yielded contrast around the tumor by adding the sequences is sufficient.

Optimization Procedure To optimize our cost function, we use SciPy's [Vir20] dual annealing approach. In addition to simulated annealing, it introduces a local search at accepted positions of the global search. We initially set the six varying parameters (three for translation and three for rotation in each direction) to zero since we assume that the segmentation position can only change slightly compared to the initial position. We set the bounds, i.e., the minimum and maximum range for each parameter, to -15 and +15 voxels for the translation parameters and -30 and +30 degrees for the rotation parameters, as, according to our medical collaborators,

larger transformations are unlikely. Following SciPy's [Vir20] documentation, the initial temperature is set to 1000, and the *visit* parameter to 1.5. These values allow for smaller search steps than the default values as we expect the optimal position to be in the close surroundings.

Cost Function To calculate the current cost, we transform the segmentation with a given parameter set **p** as determined by the dual annealing approach, yielding the transformed segmentation volume **S**. We then calculate the segmentation border area, which we refer to as the segmentation hull, by computing $\mathbf{S}_{hull} = \mathbf{S}_{dilated} - \mathbf{S}_{eroded}$ with a kernel size of 3x3x3 for the morphological operators. This slightly wider hull allows for variations of the tumor border that can occur due to varying imaging physics. Then, we extract the gradient magnitude values from the pre-processed volume **V** at the positions of the segmentation hull, smooth it with a Gaussian filter with $\sigma = 1.5$ voxels, as determined heuristically, and weigh the resulting volume by multiplying with **V** to increases the difference between low and high magnitude values. We refer to the resulting weighted volume as $\mathbf{W_p}$. We define the cost function as:

$$J(\mathbf{p}) = -2 \cdot \frac{\sum \mathbf{W_p}}{n} + \sigma(\mathbf{W_p}),$$

where n is the number of nonzero voxels of the weighted hull $\mathbf{W_p}$. **p** is the parameter vector with the translation and rotation parameters. We define a good fit as a high (first term of the cost function) and homogeneous (second term) gradient in the sequence at the borders of the transformed segmentation mask. In the first term, we compute the sum of the gray values in the weighted segmentation hull $\mathbf{W_p}$ divided by n. Since it is generally lower than the second term, we weigh it by factor 2. In the second term, we compute the standard deviation of the weighted segmentation hull $\mathbf{W_p}$ to ensure a homogeneous border.

4.2. Alignment Assessment

To assess the alignment of the segmentation mask with the individual sequences after the ASM, we propose an interactive magic lens visualization during the ISM and after registration (R3) (Figure 2). The magic lens shows the reference sequence around the current cursor position in a square. It can be used in the grid view and all slicing directions of the main view. The user can activate the magic lens and change the opacity of the overlay gradually with the keyboard. Furthermore, the segmentation mask opacity can be adapted in the toolbar. The magic lens follows the movement of the cursor. Interactions like scrolling and transformation of the segmentation are also possible while the lens is active. Furthermore, the magic lens updates based on the current segmentation transformation, which means that the translation and rotation are also applied to the magic lens (see Figure 1 for an example with slight translation and rotation compared to Figure 2). This feature enables a preview of the potential co-registration outcome and aids the alignment assessment (R3).

4.3. Interactive Shape Matching

In cases where the ASM does not lead to satisfactory results, the segmentation position can be adapted interactively by using the keyboard (R2). The transformations are then applied to the sequence under the current cursor position. The segmentation can be
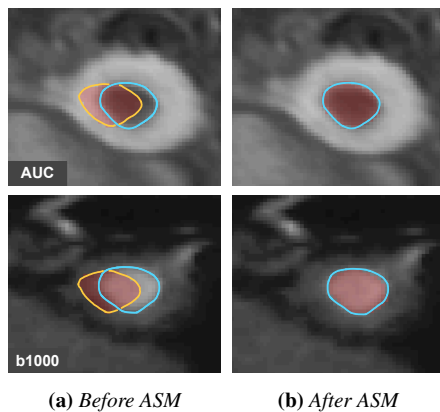
moved in four directions with the four arrow keys. Even though we represent the data in 2D, the visualization is based on a transformation of the segmentation position in 3D. The transformations are applied to the slicing direction under the cursor and affect the transformation in the other slicing directions to maintain a correct representation. Therefore, moving the segmentation to the side in the axial oblique direction might result in moving the mask back or forth in another slicing direction. The same concept applies to rotation. Several keys can rotate the segmentation around each axis at both a positive and negative angle. If the user transforms the segmentation in a sequence part of the grouping, the transformations are applied to the whole group (R4). To undo transformations, the transformation state of the segmentation can be set to its initial state.
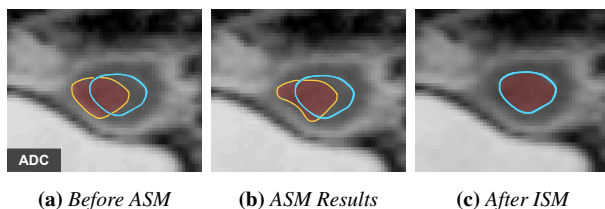
4.4. Co-Registration

We use the indices of the segmentation mask as landmarks for registration. The original indices of the reference segmentation represent the landmarks in the fixed image, while the user-adapted transformed segmentation indices are the corresponding landmarks of the moving image. To register the processed sequences to the reference sequence, we use Elastix [KSM*09] and follow the recommendations [KS18] to specify the following settings. If not specified otherwise, the default settings are used. We use a combination of the corresponding points metric (for landmark-based registration) and the advanced Mattes Mutual Information. To analyze only tumorous tissue, rigid registration would be sufficient. However, in order to take also surrounding tissue into account, especially the uterus, also deformable registration is of interest. In contrast to the tumor, the uterus is a soft structure that can be deformed based on bladder filling and intestinal movements. In deformable registration, we use a combination of rigid and B-spline transforms. We set a lower weight to the B-spline component (0.5) than the default value of 1.0 to avoid strong deformations. This setting gives a higher weight to the landmarks. We further constrain the deformable registration to the area outside the tumor with binary registration masks. These masks limit the random coordinate sampler to select voxels only in the defined area outside the tumor. We set the parameters `NewSamplesEveryIteration` and `UseRandomSampleRegion` to true. Furthermore, we use the B-spline interpolator with $N = 3$ and the adaptive stochastic gradient descent optimizer. Elastix allows for registration with both multiple fixed or moving images. We register the sequences grouped by the user as multiple moving images to the reference modality (R4). The results are shown to the user by updating the view. The segmentation position is set to its initial state (as in VIBE) and should now match the tumor borders. The alignment quality can be assessed with the help of the magic lens (R3).

5. Implementation

We used React [Wal11] for the frontend and implemented a WebGL shader written in the OpenGL ES shading language (GLSL ES) to render the sequences and segmentation data. The renderer, cameras, scenes, and objects are based on Three.js [Dan12]. We read NIfTI data in JavaScript with the open-source NIfTI reader [LM16] and facilitate backend requests with the promise-based HTTP client Axios [Zab14]. For image processing steps in the backend, we

(a) *Before ASM*　　**(b)** *After ASM*

Figure 4: *Results of the automatic shape matching (ASM) (b) in comparison to the original segmentation position (a) in two sequences with the segmentation as transparent red overlay. Blue: actual tumor borders, yellow: mismatch of the segmentation position.*

(a) *Before ASM*　　**(b)** *ASM Results*　　**(c)** *After ISM*

Figure 5: *Results of the automatic shape matching (ASM) (b) in comparison to the original segmentation position (a) in one sequence. In this case, user adaptations were necessary (c). Blue: actual tumor borders, yellow: mismatch of the segmentation position.*
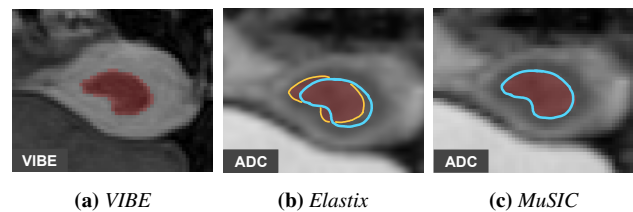
use NumPy [Oli06], and SciPy [Vir20] for Gaussian and gradient magnitude filters. Translation and rotation is carried out by SimpleITK [LCIB13]. For the automatic shape matching, we optimize the cost function by using SciPy's [Vir20] dual annealing approach. As registration framework, we use the Python interface SimpleElastix [MBSK16, KSM*09].

6. Case Studies

To demonstrate the utility of MuSIC, we examine the outcomes of the automatic shape matching and final registration results with our collaborating radiologists. Furthermore, we compare the registration outcomes of MuSIC with non-landmark-based registration. Finally, we depict examples of two patients in our data set and provide the comparison of all sequences in the additional material.

6.1. Automatic Shape Matching

In Figure 4 and Figure 5, we compare the segmentation position before and after the automatic shape matching in three different sequences of one patient. Our automatic shape matching approach can find suitable positions for the segmentation mask in PE, TTP,

(a) *VIBE*　　**(b)** *Elastix*　　**(c)** *MuSIC*

Figure 6: *Results of rigid registration with Elastix (b) and MuSIC (c) in comparison with the reference sequence VIBE (a). Blue: actual tumor borders, yellow: mismatch of the segmentation position.*

AUC, and b1000 in most cases of our data set. As mentioned in Section 4, the PE, TTP, and AUC sequences are derived and processed together in our workflow. In the ADC sequence of Patient 1 (see Figure 5), it is visually and algorithmically challenging to distinguish the tumor from the surrounding uterus tissue. Due to low contrast at the tumor border, the algorithm terminates with a cost function minimum which often represents the uterus border, where we can observe higher contrast. This phenomenon might also occur in T2 sequences or if the gray value distribution of a sequence varies from the standard range in our data set. In these cases, manual adaptations can be necessary.
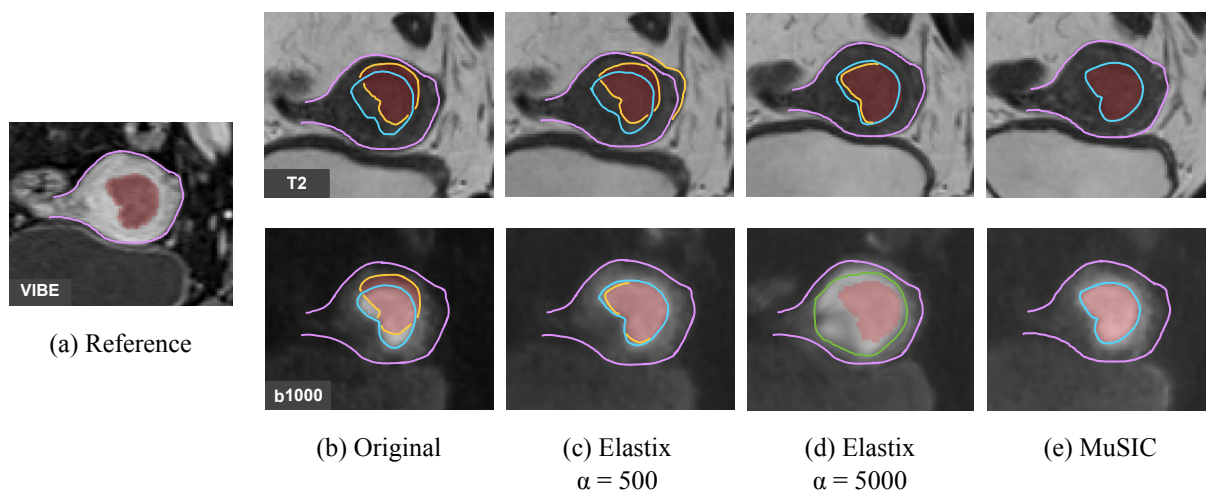
6.2. Registration

After automatic and interactive shape matching by a medical expert, we applied rigid and deformable registration to our use cases and visually compared the outcomes with non-landmark-based registration. For the latter, we used Elastix [KSM*09] and follow the settings as proposed by the Elastix manual [KS18].

Rigid Registration After performing rigid registration with MuSIC, the alignment reflects the mask positions set by the medical expert. Therefore, the results are accurate for the alignment of the tumor in all sequences. In contrast, the alignment without landmarks is often inaccurate, likely because the alignment is based on structures with high contrast, which is usually the bladder and the uterus. We show an example in Figure 6.

Deformable Registration To locally transform soft tissue surrounding the tumor, we allow for deformable registration. In this case, we are mainly interested in the alignment of the uterus and the tumor itself. We observe unnatural deformations in deformable registration without landmarks but maintaining the other settings described in Section 4. Therefore, we adapted the settings of Elastix following the manual [KS18]. We apply a higher number of iterations, 2000 instead of 500, as we use in MuSIC. Even higher values did not yield better results. Furthermore, the parameter α can be tuned that determines the amount of deformation applied to the image where higher α values allow for stronger deformations [KS18]. To adapt this parameter, we use `StandardGradientDescent` instead of `AdaptiveStochasticGradientDescent` in Elastix. We show the results of two settings ($\alpha = 500$ and $\alpha = 5000$) in Figure 7 in comparison with the outcomes of MuSIC.

Even though tumors are rigid structures, they can appear slightly

Figure 7: *Comparison of deformable registration outcomes between Elastix with two different α settings and MuSIC. Purple: shape of the uterus in VIBE as overlay over the sequences, blue: actual tumor borders, yellow: mismatch of the segmentation position or uterus border, green: unnatural deformation of the tumor.*

different in the varying sequences due to imaging physics. Therefore, applying deformable registration without landmarks can result in tumor deformations that do not resemble the underlying biological tissue characteristics and alter important tumor information. We can observe this phenomenon in the b1000 sequence in Figure 7. We can avoid these tumor deformations by using segmentation masks as landmarks, and by applying local transformations mainly to surrounding soft tissue. Additionally, we can see that a value of α = 500 sufficiently transforms the b1000 sequence (apart from minor deviations in the tumor area), while T2 would require stronger deformations. In comparison, α = 5000 aligns T2 better, but the setup applies too strong deformations in b1000. We also tested values of α between 500 and 5000, but all experiments yielded results where some sequences were transformed too much while others would have needed more substantial transformations. Furthermore, a per-sequence setup would not be sufficient, as the required settings also change between two patients. Therefore, we would have to tune the parameters for each patient and sequence individually to obtain optimal results. In contrast, according to our medical experts, the results of MuSIC are less sensitive to patient- and sequence-specific characteristics since the registration is based on matching landmarks.

7. Evaluation

To show the utility of our approach, we conducted a qualitative user evaluation with seven expert participants. M1 and M2 are radiologists and Ph.D. students in gynecological cancer research. Both were involved during the development of the application. M3 is a postdoctoral researcher with over ten years of experience in preclinical imaging. M4 is a medical physicist and Ph.D. student, and M5 is a radiographer with 12 years of experience. M1 to M5 represent the primary target audience of the application, while machine learning experts also showed interest in using the tool to co-register their data without medical experts being involved. There-

fore, we included two machine learning experts (A1 and A2). A1 is a Ph.D. student in machine learning for cancer imaging, and A2 is an associate professor of mathematics with almost 20 years of experience in the same field who also works on the automation of co-registration.

At the beginning of the evaluation, we introduced the participants to the tool and the interaction methods. Participants were encouraged to ask questions where needed. Furthermore, we asked the participants to speak out loud throughout the evaluation and let us know which features and workflows they favored and which they would change. After the introduction, the participants processed the sequences of one patient of our data set. The participants used all available features, and we further let them compare our tool to a landmark-based registration method as provided by 3D Slicer [PHK04]. We encouraged them to compare our magic lens interaction with the common checkerboard visualization offered by 3D Slicer [PHK04]. After roughly 45 minutes per person, the participants filled out a specific evaluation form about our application consisting of 23 statements and the standardized System Usability Scale (SUS) introduced by Brooke et al. [Bro04]. The 23 statements are grouped into the following categories: general statements & interaction (G1-G11), segmentation mask interaction (S1-S5), outcome evaluation (O1-O3), and comparison to 3D Slicer (traditional landmark-based co-registration) (C1-C4).

7.1. Evaluation Results

The evaluation results are presented in Table 1. Questions marked with a star were originally formulated negatively, but in the results, the scores and the questions are inverted. All participants strongly preferred our approach as an alternative to setting manual landmarks. The participants argued that it could be challenging to define landmarks in pathological data, as the tumor can appear slightly different in the various sequences due to imaging physics. Using a mask as a pre-defined landmark is a solution here. The radiolo-

Table 1: *Results of our usability analysis on a 5-point Likert scale, with meaning 1: strongly disagree and 5: strongly agree. Statements marked with a star are rephrased to the positive form in this table with inverted scores for presentation purposes. In the rightmost column, average values are presented. The last row reveals the results of the SUS questionnaire.*

	Statements	M1	M2	M3	M4	M5	A1	A2	Avg.
G1	I see myself using MuSIC in the future.	5	5	4	5	5	3	4	4,43
G2	Defining a reference view is clear and intuitive.*	5	5	5	5	5	4	5	4,86
G3	The linked slice view interactions (zooming, scrolling, moving) are intuitive.	5	2	5	5	5	5	5	4,57
G4	Reordering the sequences in the grid view is helpful to visualize related modalities next to each other.	4	4	5	5	5	4	5	4,57
G5	It is helpful to resize the sequences in the grid view.*	5	5	5	4	4	5	5	4,71
G6	Switching one sequence of the grid to the main view provides me more details when needed.	5	4	5	5	5	5	5	4,86
G7	Grouping multiple sequences is quick and intuitive.	4	5	4	5	5	4	5	4,57
G8	After grouping multiple sequences it is clear which sequences are grouped.*	5	5	5	5	4	5	5	4,86
G9	Activating and interacting with the magic lens is easy and intuitive.*	5	5	5	5	5	5	5	5
G10	The magic lens helps me to determine differences in tumor position between sequences.*	5	5	5	5	5	5	5	5
G11	It is easier to assess differences in tumor position with the integrated visualization of two sequences via the magic lens than having two sequences next to each other.	4	3	5	5	4	5	5	4,43
S1	Moving the segmentation in x, y and z direction using the keyboard is intuitive.	5	5	5	5	5	4	5	4,86
S2	Rotating the segmentation using the keyboard is intuitive.	5	5	4	5	5	5	3	4,57
S3	The possibility to change the opacity of the segmentation helps me to determine the segmentation's fit.*	5	5	4	5	5	5	5	4,86
S4	The three slicing directions in the main view help me to understand the exact position in 3D.	3	5	4	5	5	5	5	4,57
S5	It is helpful being able to reset the segmentation movement of the currently processed sequence.*	5	5	5	5	5	5	4	4,86
O1	Based on the updated slice view for each sequence and the original segmentation position, I can see if the registration is performed correctly.	5	5	5	5	5	5	5	5
O2	The magic lens is useful to check the quality of the alignment after registration.*	5	5	5	5	5	4	5	4,86
O3	It is useful to be able to further adapt the registration if needed.	5	5	5	5	5	5	5	5
C1	I prefer to process multiple sequences at a time because it is easier to keep track of differences in the tumor position.	5	5	4	5	3	4	5	4,43
C2	I think it saves time to visualize and process multiple sequences at a time.*	5	5	4	5	5	4	5	4,71
C3	It is helpful to move a predefined segmentation mask instead of setting landmarks in pathological data.	5	5	5	5	5	5	5	5
C4	I prefer the magic lens visualization over a checkerboard.*	5	5	5	5	5	5	5	5
SUS	System Usability Scale	97.5	100	97.5	100	97.5	85	90	95.4

gists also favor grouping sequences and processing them simultaneously if needed. All experts agreed on the clear structure and layout without visual overload. M5 has been using multiple tools for segmentation and registration and thinks MuSIC is very intuitive and does not have a steep learning curve. The customizable layout was rated favorably. One participant would like a clearer visualization of where to click to drag or resize a component in the customizable layout. M2 would prefer less sensitive zooming in the slice-view interactions. Generally, our participants thought the interaction with the segmentation mask via keyboard was intuitive.

The participants expressed different ideas and wishes. The images in our data set are acquired in an axial oblique direction, perpendicular to the central axis of the uterus. One of our radiologists would prefer to see the other two slicing views as real axial and sagittal slices according to the body axes (slicing from the front to the back and from left to right instead of oblique slicing), as this would be more intuitive. Furthermore, three participants would like orientation lines indicating the current position in the three slicing directions. Especially for translation, two participants expressed the

idea of additionally having mouse interaction to reduce the time needed for more extensive translations.

Our participants were enthusiastic about MuSIC and hope to use it soon to improve co-registration in their research projects. Furthermore, four of them expressed the wish to use it for not only co-registration but also for simultaneous segmentation. Currently, there are no tools available that include intuitive multi-modal segmentation visualization methods. Therefore, they mainly draw the segmentation on one of the sequences. When using our tool, however, they found that some parts of the segmentation might require adaptations because several tissue characteristics become visible throughout the various sequences. In these cases, they would strongly appreciate being able to adapt the segmentation mask.

System Usability Scores The system usability scores are shown at the end of Table 1. The lowest value is 85, and the highest value is 100. On average, our application reached a SUS of 95,4. According to Bangor et al. [BKM09] the SUS can be interpreted in three ways, the acceptability range, a grade scale like in education, and the adjective rating scale. MuSIC has an acceptance rate of Acceptable

(best possible), grade scale of A (best score), and adjective rating of Excellent (best possible score).

Among the medical experts, we achieved high SUS rating as the tool is customized to their used workflows and tooling. For our machine learning experts, this score is slightly lower. One of them thinks medical experts should perform the registration, while the one with more experience would like to use the tool himself. He states that their automated segmentation algorithms could strongly benefit from better co-registration, even if their manual segmentation fitting includes more errors than if performed by a medical expert.

7.2. Evaluation Conclusion

Overall, we received very positive feedback for our application. Considering the results from Table 1, we infer that MuSIC has the potential to be a valuable tool for multi-sequential co-registration. Our participants especially appreciated the magic lens in addition to a side-by-side view for a more detailed comparison, the outcome preview, and a final visual evaluation of the results. Gynecological cancer imaging experts and machine learning experts would like to use it in the future to enhance their data quality and enable radiomic tumor profiling research across imaging sequences.

8. Conclusion and Future Work

We present MuSIC, a web-based approach that allows radiologists to interactively co-register multi-modal cancer images by adjusting the position of pre-defined tumor segmentation masks. We propose an automatic search of the optimal segmentation positions in the other available imaging sequences by a dual annealing optimization. Users can interactively adapt the resulting positions by translating and rotating the masks. We support the user in this task with a multi-modal magic lens visualization that enables a preview of the co-registration results. Finally, we register the sequences based on the segmentation transformations and use the corresponding voxels as landmarks. We allow for both rigid and deformable registration. In contrast to existing approaches, we apply local transformations mainly outside the tumor due to our landmark-based approach, which avoids unnatural deformations and better resembles the biological conditions of a rigid tumor and surrounding soft tissue. From our usability analysis, we conclude that MuSIC can be a valuable application for improving co-registration results. Our participants especially appreciate the intuitive interface, interaction, and magic lens. Our medical experts see themselves using MuSIC in the future. The sequences used in endometrial cancer research might differ from other tumor types. However, our medical experts believe that the tool is useful for other application fields as well and the workflow is suitable for different modalities and sequences. For other data sets, we would have to adapt the settings for the automatic shape matching.

One possible line of future work could be to allow for segmentation mask adaptation or even interactive segmentation from scratch in the same environment. Furthermore, a neural network approach could replace the automatic shape matching based on dual annealing, where the segmentation masks placed by an expert user could be used as training data, for example in an active learning context.

References

[AGM17] ALIBERT C., GOUD B., MANNEVILLE J.-B.: Are cancer cells really softer than normal cells? *Biology of the Cell 109*, 5 (2017), 167–189. doi:10.1111/boc.201600078. 3

[ATS09] AVANTS B. B., TUSTISON N., SONG G.: Advanced normalization tools (ANTS). *Insight j 2*, 365 (2009), 1–35. 2

[Ber16] BERG A. E. A.: Tissue and imaging biomarkers for hypoxia predict poor outcome in endometrial cancer. *Oncotarget 7*, 43 (2016), 69844–69856. doi:10.18632/oncotarget.12004. 2, 3

[BKM09] BANGOR A., KORTUM P., MILLER J.: Determining what individual SUS scores mean: Adding an adjective rating scale. *J. Usability Studies 4*, 3 (2009), 114–123. 8

[Bro04] BROOKE J.: SUS-a quick and dirty usability scale. usability evaluation in industry. In *Usability Evaluation In Industry*. CRC Press, 2004, ch. 10, pp. 266–290. 2, 7

[BSP*93] BIER E. A., STONE M. C., PIER K., BUXTON W., DEROSE T. D.: Toolglass and magic lenses: the see-through interface. In *Proceedings of the 20th Annual Conference on Computer Graphics and Interactive Techniques* (1993), pp. 73–80. doi:10.1145/259963.260447. 3

[CK09] CHEUNG M. R., KRISHNAN K.: Interactive deformation registration of endorectal prostate MRI using ITK thin plate splines. *Academic Radiology 16*, 3 (2009), 351–357. 3

[CKMK19] CANALINI L., KLEIN J., MILLER D., KIKINIS R.: Segmentation-based registration of ultrasound volumes for glioma resection in image-guided neurosurgery. *International Journal of Computer Assisted Radiology and Surgery 14*, 10 (2019), 1697–1713. doi:10.1007/s11548-019-02045-6. 2

[CW18] CHEE E., WU Z.: Airnet: Self-supervised affine registration for 3d medical images using neural networks. *CoRR abs/1810.02583* (2018). doi:10.48550/arXiv.1810.02583. 2

[CZZ18] CHENG X., ZHANG L., ZHENG Y.: Deep similarity learning for multimodal medical images. *Computer Methods in Biomechanics and Biomedical Engineering: Imaging & Visualization 6*, 3 (2018), 248–252. 2

[Dan12] DANCHILLA B.: Three.js framework. In *Beginning WebGL for HTML5*. Springer, 2012, pp. 173–203. 5

[Dzy13] DZYUBACHYK O. E. A.: Comparative exploration of whole-body mr through locally rigid transforms. *International Journal of Computer Assisted Radiology and Surgery 8*, 4 (2013), 635–647. 3

[Fas18] FASMER K. E. E. A.: Preoperative quantitative dynamic contrast-enhanced MRI and diffusion-weighted imaging predict aggressive disease in endometrial cancer. *Acta Radiologica 59*, 8 (2018), 1010–1017. doi:10.1177/0284185117740932. 2, 3

[FLW*20] FU Y., LEI Y., WANG T., CURRAN W. J., LIU T., YANG X.: Deep learning in medical image registration: a review. *Physics in Medicine & Biology 65*, 20 (2020), 20TR01. doi:10.1088/1361-6560/ab843e. 2

[FOGM18] FERRANTE E., OKTAY O., GLOCKER B., MILONE D. H.: On the adaptability of unsupervised CNN-based deformable image registration to unseen image domains. In *International Workshop on Machine Learning in Medical Imaging* (2018), Springer, pp. 294–302. doi:10.1007/978-3-030-00919-9_34. 2

[FW01] FITZPATRICK J. M., WEST J. B.: The distribution of target registration error in rigid-body point-based registration. *IEEE Transactions on Medical Imaging 20*, 9 (2001), 917–927. doi:10.1109/42.952729. 2, 3

[GNBP11] GASTEIGER R., NEUGEBAUER M., BEUING O., PREIM B.: The FLOWLENS: A focus-and-context visualization approach for exploration of blood flow in cerebral aneurysms. *IEEE Transactions on Visualization and Computer Graphics 17*, 12 (2011), 2183–2192. doi:10.1109/TVCG.2011.243. 3

[HBR*17] HAMDAN I., BERT J., REST C. C. L., TASU J. P., BOUS-SION N., VALERI A., DARDENNE G., VISVIKIS D.: Fully automatic deformable registration of pretreatment MRI/CT for image-guided prostate radiotherapy planning. *Medical Physics 44*, 12 (2017), 6447–6455. doi:10.1002/mp.12629. 3

[HHD*21] HOIVIK E. A., HODNELAND E., DYBVIK J. A., WAGNER-LARSEN K. S., FASMER K. E., BERG H. F., HALLE M. K., HALDORSEN I. S., KRAKSTAD C.: A radiogenomics application for prognostic profiling of endometrial cancer. *Communications Biology 4*, 1 (2021), 1–12. doi:10.1038/s42003-021-02894-5. 2, 3

[HKY20] HASKINS G., KRUGER U., YAN P.: Deep learning in medical image registration: a survey. *Machine Vision and Applications 31*, 1 (2020), 1–18. 2

[Hod21] HODNELAND E. E. A.: Automated segmentation of endometrial cancer on MR images using deep learning. *Scientific Reports 11*, 1 (2021), 1–8. doi:10.1038/s41598-020-80068-9. 2

[HS16] HALDORSEN I. S., SALVESEN H. B.: What is the best preoperative imaging for endometrial cancer? *Current Oncology Reports 18*, 4 (2016), 25. doi:10.1007/s11912-016-0506-0. 1, 2, 3

[HSG*13] HALDORSEN I., STEFANSSON I., GRÜNER R., HUSBY J., MAGNUSSEN I., WERNER H., SALVESEN O., BJØRGE L., TROVIK J., TAXT T., AKSLEN L., SALVESEN H.: Increased microvascular proliferation is negatively correlated to tumour blood flow and is associated with unfavourable outcome in endometrial carcinomas. *British journal of cancer 110* (2013). doi:10.1038/bjc.2013.694. 1

[HWS*07] HANDELS H., WERNER R., SCHMIDT R., FRENZEL T., LU W., LOW D., EHRHARDT J.: 4D medical image computing and visualization of lung tumor mobility in spatio-temporal CT image data. *International Journal of Medical Informatics 76* (2007), S433–S439. doi:10.1016/j.ijmedinf.2007.05.003. 3

[JBB*12] JENKINSON M., BECKMANN C. F., BEHRENS T. E., WOOLRICH M. W., SMITH S. M.: FSL. *Neuroimage 62*, 2 (2012), 782–790. doi:10.1016/j.neuroimage.2011.09.015. 2

[JBBS02] JENKINSON M., BANNISTER P., BRADY M., SMITH S.: Improved optimization for the robust and accurate linear registration and motion correction of brain images. *NeuroImage 17*, 2 (2002), 825 – 841. doi:10.1006/nimg.2002.1132. 3

[KDSU*16] KETCHA M. D., DE SILVA T., UNERI A., KLEINSZIG G., VOGT S., WOLINSKY J.-P., SIEWERDSEN J. H.: Automatic masking for robust 3D-2D image registration in image-guided spine surgery. In *Medical Imaging 2016: Image-Guided Procedures, Robotic Interventions, and Modeling* (2016), vol. 9786, International Society for Optics and Photonics, p. 97860A. doi:10.1117/12.2216913. 2

[KK19] KORI A., KRISHNAMURTHI G.: Zero shot learning for multimodal real time image registration. *CoRR abs/1908.06213* (2019). doi:10.48550/arXiv.1908.06213. 2

[KS18] KLEIN S., STARING M.: Elastix - the manual. https://usermanual.wiki/Document/elastix490manual.1389615963/view, 2018. Last accessed: 2022-02-22. 5, 6

[KSM*09] KLEIN S., STARING M., MURPHY K., VIERGEVER M. A., PLUIM J. P.: Elastix: a toolbox for intensity-based medical image registration. *IEEE Transactions on Medical Imaging 29*, 1 (2009), 196–205. doi:10.1109/TMI.2009.2035616. 2, 5, 6

[KYWH12] KIRMIZIBAYRAK C., YIM Y., WAKID M., HAHN J.: Interactive visualization and analysis of multimodal datasets for surgical applications. *Journal of Digital Imaging 25*, 6 (2012), 792–801. doi:10.1007/s10278-012-9461-y. 3

[LCIB13] LOWEKAMP B. C., CHEN D. T., IBÁÑEZ L., BLEZEK D.: The design of SimpleITK. *Frontiers in Neuroinformatics 7* (2013), 45. 6

[LM16] LANCASTER J. L., MARTINEZ M. J.: Mango nifti-reader-js. GitHub: https://github.com/rii-mango/NIFTI-Reader-JS (accessed: 25-03-2022): Version 0.5.4., 2016. 5

[LSBP18] LAWONN K., SMIT N. N., BÜHLER K., PREIM B.: A survey on multimodal medical data visualization. In *Computer Graphics Forum*

(2018), vol. 37, Wiley Online Library, pp. 413–438. doi:10.1111/cgf.13306. 1, 3

[LXN*05] LI G., XIE H., NING H., CAPALA J., ARORA B. C., COLEMAN C. N., CAMPHAUSEN K., MILLER R. W.: A novel 3D volumetric voxel registration technique for volume-view-guided image registration of multiple imaging modalities. *International Journal of Radiation Oncology - Biology - Physics 63*, 1 (2005), 261–273. doi:10.1016/j.ijrobp.2005.05.008. 3

[Mah18] MAHAPATRA D.: GAN based medical image registration. *arXiv preprint arXiv:1805.02369* (2018). doi:10.48550/arXiv.1805.02369. 2

[MBSK16] MARSTAL K., BERENDSEN F., STARING M., KLEIN S.: SimpleElastix: A user-friendly, multi-lingual library for medical image registration. In *Proceedings of the IEEE Conference on Computer Vision and Pattern Recognition Workshops* (2016), pp. 134–142. https://simpleelastix.github.io (accessed: 19-04-2022). 2, 6

[MEH*22] MÖRTH E., EICHNER T., HALDORSEN I., BRUCKNER S., SMIT N.: ICEVis: Interactive clustering exploration for tumor subregion analysis in multiparametric cancer imaging. *15th International Symposium on Visual Information Communication and Interaction (VINCI'22)* (2022). doi:10.1145/3554944.3554958. 2

[MHG10] MALIK M. M., HEINZL C., GROELLER M. E.: Comparative visualization for parameter studies of dataset series. *IEEE Transactions on Visualization and Computer Graphics 16*, 5 (2010), 829–840. doi:10.1109/TVCG.2010.20. 3

[MLC*16] MORICE P., LEARY A., CREUTZBERG C., ABU-RUSTUM N., DARAI E.: Endometrial cancer. *The Lancet 387*, 10023 (2016), 1094–1108. doi:10.1016/S0140-6736(15)00130-0. 1

[MR] MIKHEEV A., RUSINEK H.: Firevoxel. https://firevoxel.org. Last accessed: 2022-03-07. Radiology Department, NYU School of Medicine. 3

[Mun09] MUNZNER T.: A nested model for visualization design and validation. *IEEE Transactions on Visualization and Computer Graphics 15*, 6 (2009), 921–928. 3

[MV98] MAINTZ J. A., VIERGEVER M. A.: A survey of medical image registration. *Medical Image Analysis 2*, 1 (1998), 1–36. doi:10.1016/S1361-8415(01)80026-8. 2

[MWLH*20] MÖRTH E., WAGNER-LARSEN K., HODNELAND E., KRAKSTAD C., HALDORSEN I. S., BRUCKNER S., SMIT N. N.: RadEx: Integrated visual exploration of multiparametric studies for radiomic tumor profiling. In *Computer Graphics Forum* (2020), vol. 39, Wiley Online Library, pp. 611–622. doi:10.1111/cgf.14172. 2

[Oli06] OLIPHANT T. E.: *A guide to NumPy*, vol. 1. Trelgol Publishing USA, 2006. 6

[PHK04] PIEPER S., HALLE M., KIKINIS R.: 3D Slicer. In *2nd IEEE International Symposium on Biomedical Imaging: Nano to Macro* (2004), IEEE, pp. 632–635. 3, 7

[PMEM16] PLUIM J. P., MUENZING S. E., EPPENHOF K. A., MURPHY K.: The truth is hard to make: Validation of medical image registration. In *International Conference on Pattern Recognition (ICPR)* (2016), pp. 2294–2300. doi:10.1109/ICPR.2016.7899978. 2, 3

[PMWH05] PLUEMPITIWIRIYAWEJ C., MOURA J. M., WU Y.-J. L., HO C.: STACS: New active contour scheme for cardiac mr image segmentation. *IEEE transactions on medical imaging 24*, 5 (2005), 593–603. 2

[RS14] RUECKERT D., SCHNABEL J. A.: *Registration and Segmentation in Medical Imaging*. Springer, 2014, pp. 137–156. doi:10.1007/978-3-642-44907-9_7. 2

[SDP13] SOTIRAS A., DAVATZIKOS C., PARAGIOS N.: Deformable medical image registration: A survey. *IEEE Transactions on Medical Imaging 32*, 7 (2013), 1153–1190. doi:10.1109/TMI.2013.2265603. 2

[SFF06] SCHUMACHER H., FRANZ A., FISCHER B.: Weighted medical image registration with automatic mask generation. In *Medical Imaging 2006: Image Processing* (2006), vol. 6144, SPIE, pp. 740–747. `doi:/10.1117/12.651323`. 2

[SFJ*16] SCHLACHTER M., FECHTER T., JURISIC M., SCHIMEK-JASCH T., OEHLKE O., ADEBAHR S., BIRKFELLNER W., NESTLE U., BÜHLER K.: Visualization of Deformable Image Registration Quality Using Local Image Dissimilarity. *IEEE Transactions on Medical Imaging 35*, 10 (2016), 2319–2328. `doi:10.1109/TMI.2016.2560942`. 3

[SGBM*16] SIMONOVSKY M., GUTIÉRREZ-BECKER B., MATEUS D., NAVAB N., KOMODAKIS N.: A deep metric for multimodal registration. In *International Conference on Medical Image Computing and Computer-Assisted Intervention* (2016), Springer, pp. 10–18. 2

[SHS*14] SMIT N. N., HANEVELD B. K., STARING M., EISEMANN E., BOTHA C. P., VILANOVA A.: RegistrationShop: An interactive 3D medical volume registration system. In *Eurographics Workshop on Visual Computing for Biology and Medicine* (2014). `doi:10.2312/vcbm.20141193`. 3

[SZ18] SUN L., ZHANG S.: Deformable MRI-ultrasound registration using 3D convolutional neural network. In *Simulation, Image Processing, and Ultrasound Systems for Assisted Diagnosis and Navigation*. Springer, 2018, pp. 152–158. 2

[TA13] TAVAKOLI V., AMINI A. A.: A survey of shaped-based registration and segmentation techniques for cardiac images. *Computer Vision and Image Understanding 117*, 9 (2013), 966–989. `doi:10.1016/j.cviu.2012.11.017`. 2

[TYW*03] TSAI A., YEZZI A., WELLS W., TEMPANY C., TUCKER D., FAN A., GRIMSON W. E., WILLSKY A.: A shape-based approach to the segmentation of medical imagery using level sets. *IEEE Transactions on Medical Imaging 22*, 2 (2003), 137–154. `doi:10.1109/TMI.2002.808355`. 2

[Vir20] VIRTANEN P. E. A.: SciPy 1.0: Fundamental algorithms for scientific computing in Python. *Nature Methods 17* (2020), 261–272. `doi:10.1038/s41592-019-0686-2`. 4, 5, 6

[VLM*17] VANDAELE R., LALLEMAND F., MARTINIVE P., GULYBAN A., JODOGNE S., COUCKE P., GEURTS P., MARÉE R.: Automated multimodal volume registration based on supervised 3D anatomical landmark detection. *SciTePress Digital Library* (2017). `doi:10.5220/0006153803330340`. 2

[Wal11] WALKE J.: React.js. `https://reactjs.org` (accessed: 24-05-2022), 2011. 5

[XN19] XU Z., NIETHAMMER M.: DeepAtlas: Joint semi-supervised learning of image registration and segmentation. In *International Conference on Medical Image Computing and Computer-Assisted Intervention* (2019), Springer, pp. 420–429. `doi:10.48550/arXiv.1904.08465`. 2

[Zab14] ZABRISKIE M.: Axios: A promise-based HTTP client. `https://axios-http.com` (accessed: 19-04-2022). Version 0.21.4., 2014. 5

[ZRC*20] ZAKARIA M. A., RAJAB N. F., CHUA E. W., SELVARAJAH G. T., MASRE S. F.: The roles of tissue rigidity and its underlying mechanisms in promoting tumor growth. *Cancer Investigation 38*, 8-9 (2020), 445–462. `doi:10.1080/07357907.2020.1802474`. 3